BJR

https://doi.org/10.1259/bjr.20180326

Received: 08 April 2018 | Revised: 05 June 2018 | Accepted: 07 June 2018

Cite this article as:
Chandrasekharan P, Tay ZW, Zhou XY, Yu E, Orendorff R, Hensley D, et al. A perspective on a rapid and radiation-free tracer imaging modality, magnetic particle imaging, with promise for clinical translation. *Br J Radiol* 2018; **91**: 20180326.

REVIEW ARTICLE

A perspective on a rapid and radiation-free tracer imaging modality, magnetic particle imaging, with promise for clinical translation

[1]PRASHANT CHANDRASEKHARAN, PhD, [1]ZHI WEI TAY, PhD, [1]XINYI YEDDA ZHOU, BS, [2]ELAINE YU, PhD, [2]RYAN ORENDORFF, PhD, [2]DANIEL HENSLEY, PhD, [1]QUINCY HUYNH, MS, [1]K. L. BARRY FUNG, BASc, [1]CAYLIN COLSON VANHOOK, BS, [2]PATRICK GOODWILL, PhD, [1]BO ZHENG, PhD and [1,3]STEVEN CONOLLY, PhD

[1]Department of Bioengineering, University of California, Berkeley, CA, USA
[2]Magnetic Insight Inc, Alameda, CA, USA
[3]Department of Electrical Engineering and Computer Sciences, University of California, Berkeley, CA, USA

Address correspondence to: Dr Prashant Chandrasekharan
E-mail: *prashantc@berkeley.edu*

†The authors Prashant Chandrasekharan and Zhi Wei Tay contributed equally to the work.

ABSTRACT

Magnetic particle imaging (MPI), introduced at the beginning of the twenty-first century, is emerging as a promising diagnostic tool in addition to the current repertoire of medical imaging modalities. Using superparamagnetic iron oxide nanoparticles (SPIOs), that are available for clinical use, MPI produces high contrast and highly sensitive tomographic images with absolute quantitation, no tissue attenuation at-depth, and there are no view limitations. The MPI signal is governed by the Brownian and Néel relaxation behavior of the particles. The relaxation time constants of these particles can be utilized to map information relating to the local microenvironment, such as viscosity and temperature. Proof-of-concept pre-clinical studies have shown favourable applications of MPI for better understanding the pathophysiology associated with vascular defects, tracking cell-based therapies and nanotheranostics. Functional imaging techniques using MPI will be useful for studying the pathology related to viscosity changes such as in vascular plaques and in determining cell viability of superparamagnetic iron oxide nanoparticle labeled cells. In this review article, an overview of MPI is provided with discussions mainly focusing on MPI tracers, applications of translational capabilities ranging from diagnostics to theranostics and finally outline a promising path towards clinical translation.

INTRODUCTION

Magnetic particle imaging (MPI), first invented by Gleich and Weizenecker in 2005,[1] is a breakthrough in medical imaging with great potential for clinical translation. While the first generation of scanners were home-built,[2–5] commercial preclinical scanners from Bruker BioSpin GmbH (Germany) and Magnetic Insight Inc (USA) have become available. Researchers and clinicians alike are exploring ways for extending the horizon of applications of this safe, sensitive and non-radioactive tracer modality. MPI is a tracer modality and "sees" superparamagnetic iron oxide nanoparticles (SPIOs). MPI, unlike MRI or X-ray CT does not acquire anatomical information. MPI generates positive signals from only at the position of SPIO without any discernible background tissue signal. This property of MPI is particularly useful in acquiring tomographic images at any depth without signal attenuation from bones, tissue air gap, or even soft tissue, as a result, MPI produces high contrast, highly sensitive (~100 nM of iron) and linearly quantitative images even in visceral spaces of lung and gastrointestinal tract.

SPIOs are ensemble of ferromagnetic nanoscale particle that has a net "high" magnetization when exposed to a magnetic field and a net "zero" magnetization on removing the external magnetic field, hence these are called *superparamagnetic*. In MPI, a free-field region (FFR) is created using gradient magnets (Figure 1). The FFR is rastered across in space and the SPIOs that come under the influence of the FFR, flip instantaneously, inducing a voltage based on Faraday's law of induction, which gets picked up by sensitive coils. With knowledge of the instantaneous FFR location, an image is simply reconstructed by temporospatially mapping the signal of SPIOs[8,9] (Figure 1). Image

Figure 1. MPI (A) a 6.3 T m^{-1} vertical bore FFL small animal imaging MPI scanner at UC Berkeley (reproduced with permission from[6]), (B) MPI scanner produces a gradient field as shown with a FFP or FFR and saturating regions. The FFR can be electromagnetically shifted around in space. (C) SPIOs have net zero magnetization at room temperature without any external magnetic field, however, with the applied magnetic field SPIOs magnetize and saturate. Only SPIOs at the FFR can respond to excitation, thereby localizing the signal in space, while SPIOs in other regions are saturated. This figure shows an 1-D example, the magnetization of the SPIO changes rapidly as the FFR is shifted and moved over the SPIO, therefore generating a sharp inductive signal ($s(x_s(t))$. When two SPIOs are present, two signal peaks are generated. The timing of the peak can be spatiotemporally mapped into location of the SPIO by knowledge of FFR position in time. (Image reproduced with permission from[7]) (D) To form an image we raster the FFR in space along the typical trajectory as shown (E) A 3D UC/Cal phantom filled with SPIOs[7] imaged using a projection MPI scanner. (F) Experimental demonstration of magnetic CT using a FFL scanner and projection reconstruction. 3D MPI scan of Cal/ UC phantom resolving 2D plane of Cal (TOP) and UC (Bottom). Berkeley image reconstruction algorithms enable sharp, isotropic resolution MPI images (Image reproduced with permission from[3]). 1D, one-dimensional; 2D, two-dimensional; 3D, three-dimensional; FFL, field-free line; FFP, field-free point; FFR, field-free region; MPI, magnetic particle imaging; SPIO, superparamagnetic iron oxide nanoparticle.

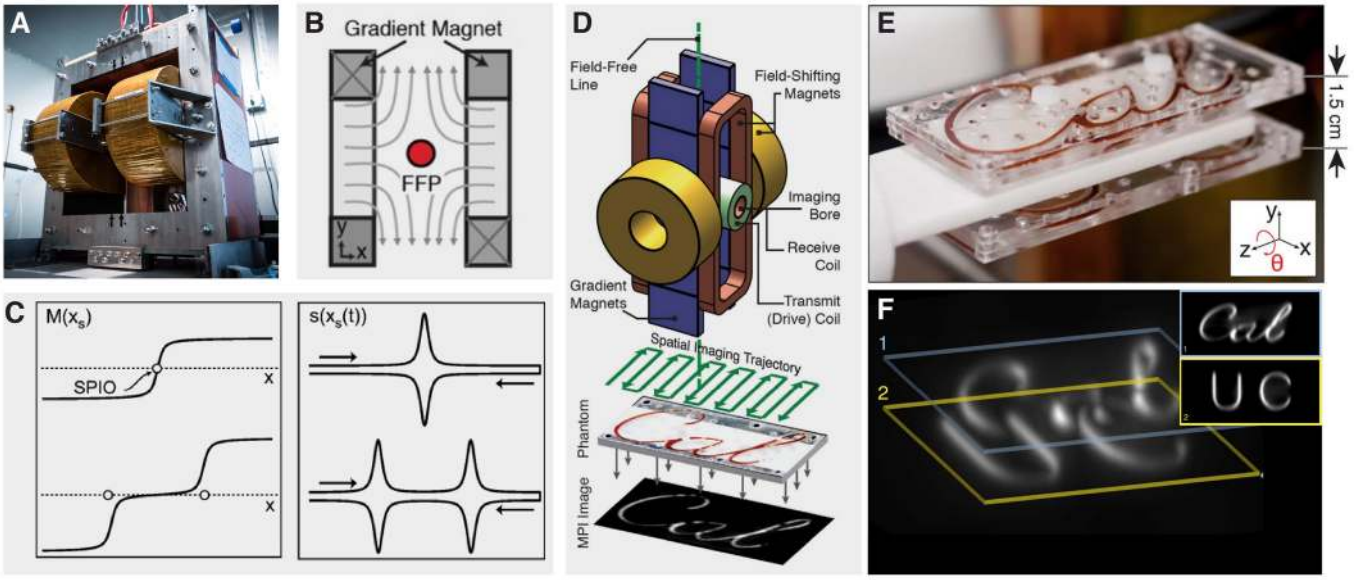

acquisition and reconstruction are detailed in papers from Gleich & Weiznecker,[1] Goodwill & Conolly[10,11] and Rahmer et al.[12]

MPI tracers are non-radioactive and their signal does not decay over time. MPI, like nuclear medicine, is a tracer functional imaging modality useful for diagnosis of pathologies associated with vascular defect, detecting changes in local microenvironment of tissues, imaging receptor-ligand interaction and *in vivo* cell tracking. The non-radioactive MPI tracer enables safe labeling and long-term tracking of cell based therapeutics.[5]

In this review, we will first introduce the properties of MPI tracers, their current market status and use. Next, we will highlight certain applications of clinical relevance. Finally, we will discuss clinical translation and future prospects of MPI.

MPI TRACERS

MPI is a tracer modality that relies on nanosized iron oxide nanoparticles with characteristic superparamagnetic behavior. As early as 1957, the first report of the use of iron oxide particles for clinical applications was demonstrated.[13] The earliest development of iron oxide nanoparticles for the diagnostic purpose was to image the reticuloendothelial system (RES) using MRI. SPIOs are made of Fe_2O_3 or Fe_3O_4 crystals of iron oxide, which are colloidally stabilized using biocompatible materials such as carboxydextran or polyethylene glycol (PEG) and reconstituted in pharmaceutical adjuvant for intravenous administration. The superparamagnetic behavior of SPIOs is attributed to the size of the particle being confined to a single domain. As explained earlier, the SPIOs have zero remanence and coercivity. For MPI, the signal is governed by the saturation magnetization of the particle, while the slope of the Langevin curve influences the image resolution. Upon application of external magnetic field, the dynamics of SPIO magnetization is influenced by the relaxation time constant. The relaxation of SPIO is influenced by two time constants, the Néel time constant τ_N and the Brownian time constant τ_B, which results in net relaxation of $\tau^{-1} = \tau_N^{-1} + \tau_B^{-1}$. The Néel time constant refers to the time for the internal magnetic moment to align with the external magnetic field which is affected by the interdomain interaction within the particles, whereas the Brownian time constant defines the rotational time that the entire particle goes through with respect to the external magnetic field and is affected by the local microenvironment. According to the Langevin model of superparamagnetism, the spatial resolution should improve cubically with the magnetic core diameter, however, Tay ZW et al[14] demonstrated that the image resolution improvement in larger core particles is limited as result of Brownian relaxation blurring. Tay ZW et al demonstrated an ideal core diameter of 24 nm yielded the best MPI image

resolution of ~3 mm at a gradient strength of 3.5 T m^{-1}. In Table 1, we have summarized properties of some of the commercially available SPIO and their MPI resolution and sensitivity estimate at a gradient strength of 7 T m^{-1}. It can be observed from Table 1, that larger core size or clustered core particles showed better resolution and sensitivity when compared to smaller core particles of Feraheme™ or NC10015.

As mentioned earlier, the relaxation time constant influences the signal in MPI. The relaxation behavior of the SPIOs can, thus, be exploited to measure changes in the local environment of the particle.[21] Utkur M et al, utilized the SPIO relaxation time constant to map the viscosity using MPI.[22] In another work, John Weaver correlated the time constant τ as a monotonic function of temperature and thus, introduced a concept for measuring the temperature of the local environment surrounding the SPIO.[23] Stehning et al demonstrated in *vitro* colorization of MPI signal based on the SPIO temperature.[24] Rahmer et al and Hensley et al devised a mechanism, termed color MPI, to unmix MPI signal from a mixture of SPIO based on the dominant relaxation behavior that the particle exhibit, *i.e.* Néel or Brownian and generate relaxation maps of the MPI signal corresponding to the particles.[25,26] In a different approach, Rahmer et al, applied the principle of color MPI to stain a blood vessel phantom and catheter differentially, and using real-time multicolor MPI feedback, Rahmer was able to steer the catheter through a vessel phantom with the use of an external magnetic field.[27]

Unlike ionic contrast agents, SPIOs have low osmolality and are safe for use with patients having renal insufficiency. The iron core of the tracer used in MPI is safe for use and assimilated and excreted via the hepatobiliary system. In one study, iron oxide nanoparticles were shown to be assimilated and incorporated into the porphyrin rings of hemoglobin.[28,29] In the same study, the rodents tolerated iron oxide concentration of up to 3000 μmol Fe kg^{-1}. A Phase I clinical study of Ferucarbotran dose demonstrated a safe use of the tracer at doses of 5–40 μmol of Fe kg^{-1}. We note that there was a single case of anaphylactic reaction in this study.[30] However, the anaphylactic response was attributed to immune response to the dextran coating of the nanoparticles.[31]

The size and surface coating of the SPIO, influence the pharmacokinetics behavior and the biodistribution of the particles in *vivo*.[32] Keselman P et al studied the biodistribution of carboxydextran and PEG-modified SPIO using MPI.[19] While the carboxydextran coated iron oxide nanoparticles cleared rapidly to the liver, the PEG-modified SPIOs had a relatively long blood half-life of 4.2 h before, eventual uptake by the RES system (liver and spleen) (Figure 2). The choice of SPIO and surface coating influence the potential diagnostic applications using MPI. A blood pool agent is useful in studying vascular defects,[6] whereas particles coated with carboxydextran are useful for imaging the liver[34] due to RES targeting or for labeling cells for long-term tracking.[5,35]

Current SPIOs that are available for clinical use are Resovist™ (Japan for MRI), Nanotherm™ (Germany for Magnetic Hyperthermia), Feraheme™ (North America, for iron supplement therapy in anemic patients) and Sienna+ (Europe, for lymph node localization). Other SPIOs are continued to be used for iron supplement therapy in anemic candidates,[36,37] as a T1 agent for MRI angiography,[38,39] as agents for diagnosis of liver cancers[40,41] and lymph node metastases with MRI.[42,43] We detail a few of these agents and their MPI performance in Table 1. Many clinicians and researchers are optimistic to resuscitate some SPIO agents that did not get prior regulatory approval. In one such process, clinicians from Radbound University Medical center, Netherlands, obtained the license to prepare and use Combidex™ (ferumoxtran-10) and evaluated its diagnostic value in the detection of small lymph node metastases in the prostate cancer patient. The authors reported identifying lymph node as small as 1.5 mm (current resolution limit of MPI) with an excellent safety profile.[44]

As the SPIO tracer defines the image resolution and sensitivity in MPI, extensive work is required in SPIO chemistry and nanoscale physics to optimize new SPIOs for MPI. Moreover, SPIO coatings can be altered to tailor their biochemical properties to the physiological application. Subsequently, these MPI-optimized SPIOs will have to undergo regulatory evaluation before being clinically available. Regardless, this is a necessary enabling step for the many emerging clinical applications of MPI and we believe that the numerous MPI nanoparticle research groups around the world are making progress towards this goal.

CLINICALLY RELEVANT APPLICATIONS OF MPI

Perfusion imaging

Perfusion imaging is a technique in which the passage of the tracer is monitored continuously through the capillary bed of tissue, capturing the temporal changes of the tracer. Perfusion imaging has long been used for diagnosis and risk stratification of stroke, grading of tumors, estimating blood–brain barrier permeability, and evaluation of various other pathophysiologies related to vascular changes. MPI is particularly advantageous for perfusion imaging due to *zero background signal, higher sensitivity, and linearity* in quantifying the SPIO concentration. As such, MPI enables direct imaging of the perfusion.

One application of perfusion imaging is in the lungs, which is needed for diagnosis of common conditions such as pulmonary embolism, a critical condition requiring time-sensitive detection and treatment. Zhou X et al reported the first MPI-based lung perfusion study using[45] macroaggregated albumin conjugated to SPIOs (MAA-SPIOs). This type of study is traditionally accomplished using scintigraphy with Tc99m-MAA. Intravenously administered, these MAA-SPIO complexes get trapped in the lung capillary bed, enabling diagnosis of any vascular related pulmonary defects. These were eventually cleared safely from the lungs to liver and spleen for degradation, showing promising biocompatibility of these agents for non-invasive lung perfusion studies (Figure 3).

Stroke occurs due to interrupted blood supply to the brain and can be deadly if not diagnosed and treated promptly. Ludewig et al developed a middle cerebral artery occlusion (MCAO) model in

Table 1. Various iron oxide contrast agent and their MPI performance measured using our MPS

Iron oxide	Marketing status	Applications	Core diameter/ hydrodynamic diameter (nm)	FWHM [a](Δx) in mT	FWHM [b](Δx) in mm	MPI sensitivity [a](V/g of Fe)	MPI sensitivity[c] [d] (ng of Fe)	References
Resovist® Bayer	Approved for clinical use in EU/ Japan	Liver imaging using MRI	**3–5 clustered/62**	**9.6**	**1.37**	**13.74**	**11.9**	[15]
Feraheme® AMAG Pharma	Approved for use by the FDA	Iron replacement therapy/ MR angiography	**6–7**/28–32	**39.5**	**5.64**	**2.12**	**77.22**	[16,17]
NC100150/PEG Feron (Research Grade)	Removed from market	Blood pool agent for MRI	**5–7/20**	**102.7**	**14.5**	**0.35**	**467.74**	[18]
VivoTrax™	Research use only	Liver imaging using MRI & MPI	**4.2/62**	**11.4**	**1.63**	**8.83**	**18.54**	[19]
LodeSpin Lab (LS017)	Research use only	Optimized MPI tracer for blood pool imaging using MPI	**28.7/89.3**	**5.8**	**0.83**	**54.57**	**3.00**	[6]
FeraSpinXXL	Research use only	Blood pool imaging using MRI	**Clustered/60–70**	**9.0**	**1.28**	**25.22**	**6.49**	–
Micromod Perimag™	Research use only	MRI agent	**Clustered/130**	**7.3**	**1.04**	**29.49**	**5.55**	–
Imagion Biosystems PrecisionMRX® (24.4 nm particles)	Research use only	MRI/MPI agent	**24.4 (monodisperse) / 41**	**12.4**	**1.77**	**13.89**	**11.7**	[14]

FDA, Food and Drug Administration; FWHM, full width at half maximum; MPI, magnetic particle imaging.

[a]The measurements reported were carried out using a magnetic particle spectrometer/relaxometer (MPS) where the device and operation are detailed in prior work.[20]

[b] Spatial resolution is calculated using the Houston criterion, and the full width at half maximum (FWHM) resolution was derived from the point spread function of the sample measured at 20 mT with 20 kHz excitation field. The gradient value used was 7 T/m. Resolution (Δx in mm) = FWHM in mT divided by scanner gradient strength in T m^{-1}.

[c]Calculations for sensitivity was based on comparison of the sensitivity of various samples on the MPS *vs* the LS017 sensitivity in the MPS and the derived sensitivity ratios were converted to absolute values by referencing the three ng per voxel sensitivity reported for LS017 in prior in vivo work.[6] (voxel size was 0.1 × 0.2 cm projected over 4 cm in the third dimension).

[d]Device detection limit based on LS017 was 163.71 nV; The sensitivity of other particles were calculated based on the device sensitivity for LS017 (in nV) divided by individual particle sensitivity in (V/g).

Figure 2. MPI tracers core size and the surface coating play a crucial role in determining the biodistribution and pharmacokinetic behavior of the particles. The figure shows TEM images of the tracers (A) LodeSpin labs (LS017) (Adapted with permission from Yu E et al.,,[6] Copyright 2017 American Chemical Society) and (B) Resovist® (Bayer-Schering). LodeSpin particles are of single core 28 nm size particle coated and stabilized with PEG, resulting in a hydrodynamic diameter of 89 nm. Resovist® is multicore MPI agents having a conglomerate of iron oxide particles, and coated with carboxydextran. Resovist has a core iron oxide diameter of 5 nm and hydrodynamic diameter of 60 nm. (C) (TOP) MPI response of Resovist™ and optimized nanoparticles of LodeSpins (UW-2), the PSF shows the LodeSpins particle have six times the intensity and two times better resolution than Resovist™ (BOTTOM) the spectrum demonstrates greater harmonics for LodeSpins particles than Resovist™ (Image reproduced with permission from[33]) (Table 1 details the sensitivity and FWHM of various SPIOs calculated from the PSF measurement). The surface coating and the size of the core determine the biodistribution of the SPIO tracer. (D) MPI image of a rodent co-registered with a projection X-ray anatomy image demonstrate carboxydextran coated iron oxide nanoparticle such as Resovist® are taken up by the RES system while (E) PEG coated particles of LodeSpins have a longer blood circulation and behave as blood pool agents (Adapted with permission from Keselman P et al[19] Institute of Physics and Engineering in Medicine. IOP Publishing). FWHM, full width at half maximum; MPI, magnetic particle imaging; MPS, magnetic particle spectrometer; PEG, polyethylene glycol; PSF, point spread function; TEM, transmission electron microscopy.

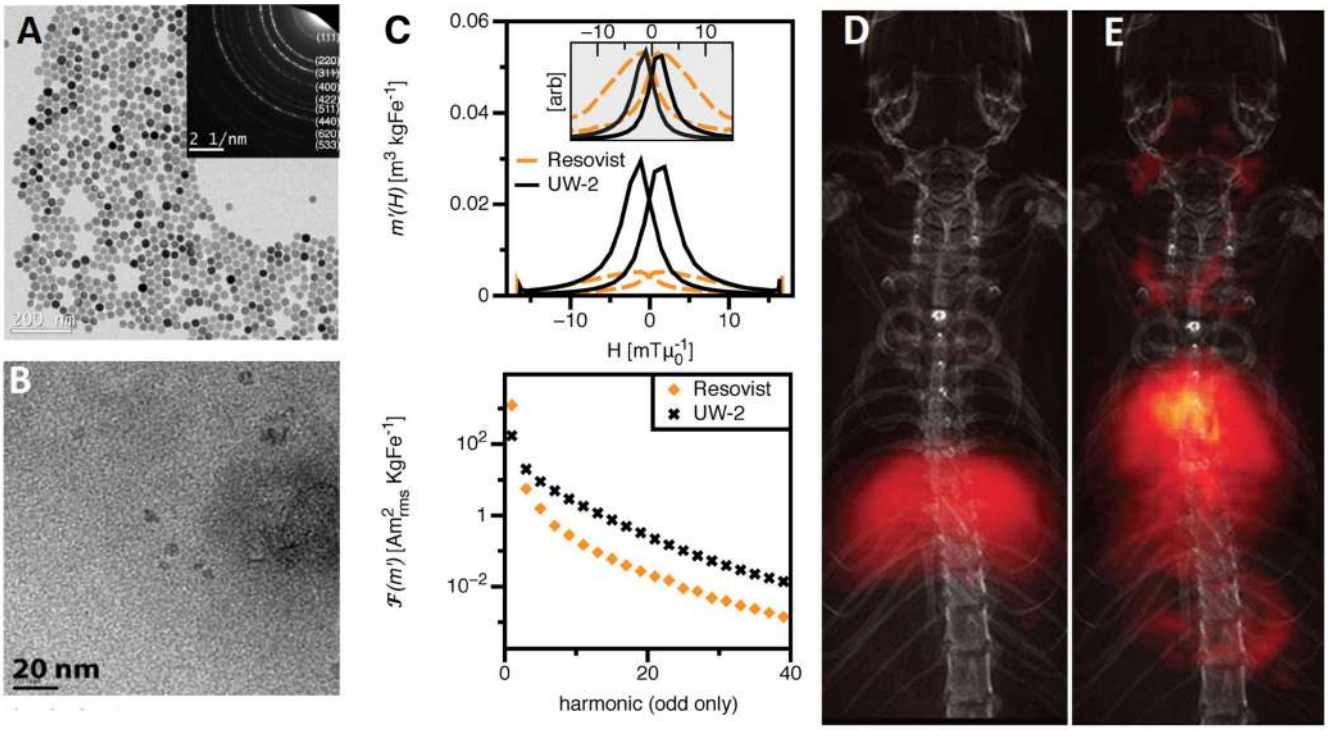

rodents and demonstrated the use of cerebral blood perfusion (CBF) with high temporal resolution, capturing three-dimensional MPI volumes at 47 frames per second for early detection of ischemic stroke.[46] Figure 3 shows that the rCBF estimate is lower in the side of the brain having an ischemic lesion, whereas the contralateral side of the brain was well-perfused.

In another study, Yu E et al estimated tracer extravasation in the gastrointestinal lumen as result of acute bleeding.[6] Conventionally, this is achieved using scintigraphy techniques in which the red blood cell (RBC) is tagged using a radioisotope such as Tc99m or In111, but because gastrointestinal bleed is often a medical emergency requiring timely diagnosis and intervention, the long (2–3 h.) hot chemistry preparation time of 99m-Tc-RBCs may not be ideal. Yu E et al used long circulating SPIOs that can be injected without hot chemistry preparation time and acquired dynamic MPI projection images showing competitive acute bleed detection sensitivity with ^{99}m-Tc-RBC. With digital subtraction, it was further possible to quantify the gastrointestinal bleed using simple tracer kinetic modeling and rates as slow as 1–5 μl min^{-1} could be detected (Figure 3). MPI, with its linearly quantitative nature, is thus promising for imaging and staging of pathophysiologies related to blood perfusion while avoiding typical hindrances such as hot chemistry labeling and background tissue signal interference.

Another area of interest for medical imaging is cancer detection and staging. Enhanced permeability and retention (EPR) is a phenomenon observed in cancer because of neoangiogenesis resulting in disorderly and chaotic vasculature that is predominantly leaky.[47] Nanoparticles and macromolecules are believed to accumulate in tumors due to EPR. Various anticancer nanotherapeutics have been developed exploiting EPR and it is essential to identify cancer patients who are most likely to respond to each nanomedicine type.[48] Yu E et al demonstrated the EPR phenomenon using MPI in a triple negative human breast

Figure 3. MPI for measuring perfusion changes. (A) First in *vivo* MPI lung perfusion studies using SPIOs modified with macro-aggregated albumin. The particles pass through the lung capillaries at 15 min and slowly get cleared to the liver. MPI is useful for imaging the lungs, where other imaging modalities tend to fail (Image adapted from Zhou X et al[45] Institute of Physics and Engineering in Medicine. Adapted with permission of IOP Publishing.) (B) First brain perfusion study performed by Ludewig et al in a rodent stroke model. The rCBF parametric estimate show reduced perfusion of blood in the parts of the brain affected by stroke, however, the contralateral side appears well perfused (Adapted with permission from Ludewig P et al[46] Copyright 2017, American Chemical Society). (C) Images show the first *in vivo* MPI gut bleed detection using long-circulating MPI tracer. The tracer accumulates in the GI lumen with time due to the occurrence of an acute bleed (Adapted with permission from Yu E et al[6] 2017 Copyright, American Chemical Society). CBF, cerebral blood perfusion; GI, gastrointestinal; MPI, magnetic particle imaging; SPIOs, super paramagnetic iron oxide nanoparticles.

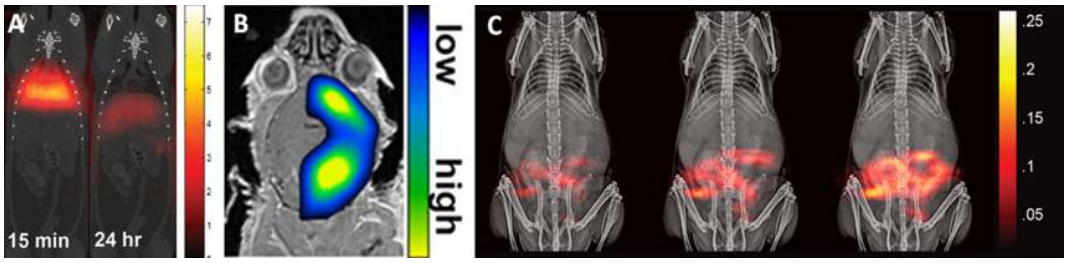

cancer xenograft in an immune deficient rodent model.[49] The MPI images using (Figure 4) a long-circulating SPIO gave excellent visualization of EPR wash-in of SPIOs into the tumor with delayed wash-out at 48 h later. The study revealed that the tumors were well-perfused in the tumor periphery, whereas the tumor core was poorly perfused.

MPI angiography

One highly compelling application of MPI would be for safe angiography in patients with renal insufficiency and in pediatric cases to minimize exposure to toxic ionic metal chelates. Each gadolinium-based radiologic study has been associated with a 2.4% risk for nephrogenic systemic fibrosis,[50] and an increased mortality rate was observed with iodine contrast exposure in patients with acute renal insufficiency.[51] MPI angiography can be achieved with good sensitivity and contrast using long circulating SPIOs that are predominantly cleared via the hepatobiliary route. MPI angiograms can be useful for diagnosis of deep vein thrombosis, evaluation of cardiovascular defect and restenosis. One of the key applications of MPI angiography is for the assessment of an aneurysm in the brain and cardiac angiogram. Jan Sedlacik et al demonstrated using a Bruker BioSpin GmbH pre-clinical MPI scanner and a four-dimensional flow imaging technique, that enabled the temporal and spatial evolution of three-dimensional blood flow (Figure 5) , capturing high-resolution pulsatile blood flow images with blood velocity of 60 cm s^{-1}.[52] Lu K et al in her work detailing the property of linear and shift invariant of MPI scanners, used carotid artery phantoms to show vascular stenosis and was able to resolve occlusion (Figure 5) at high resolution and detailed the linear quantitative nature of MPI.[53]

Another method to achieve long circulation for angiography is to load RBCs with SPIOs.[55] Rahmer J et al[56] used this method to capture cardiovascular images in a murine model with temporal resolution of 21.5 ms. Such SPIO labeled RBCs can be useful for other applications as well. For example, these can be used in the non-radioactive diagnosis of vascular defects and quantification of gastrointestinal bleeds as described earlier.[6]

MPI cell tracking

MPI has significant advantages for tracking of cells. Cell-based diagnostics are typically used with scintigraphy for non-invasive

Figure 4. First MPI perfusion studies in a tumor xenograft. The tracer distribution in the tumor over the course of time reveal well-perfused tumor periphery and poorly perfused tumor core. The MPI tracer distributes in the tumor and is cleared eventually (Images adapted with permission from Yu E et al[49] 2017 Copyright, American Chemical Society). MPI, magnetic particle imaging.

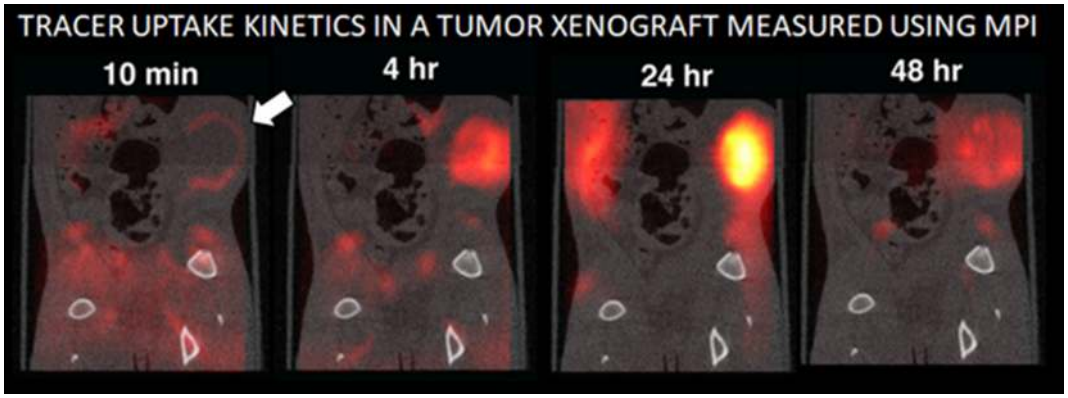

Figure 5. MPI angiograms. (A) A 4D flow image of aneurysm phantom obtained by Sedlacik J et al using a Bruker BioSpin GmbH preclinical MPI scanner (Reproduced under creative commons attribution license from[52]), the part of the phantom having aneurysm shows a decreased flow rate. (B) MPI angiogram showing a stenosis (50% occlusion) in an internal carotid artery phantom obtained by Lu K et al from University of California Berkeley (Adapted with permission from Lu K et al[53] IEEE) . (C) MPI angiogram of a rodent head showing blood vessels constituting to the CBV acquired using a FFP scanner at UC Berkeley (Reproduced with permission for Zheng B et al[54] Copyright Springer Nature). 4D, four-dimensional; CBV, cerebral blood volume; FFP, field-free point; MPI, magnetic particle imaging.

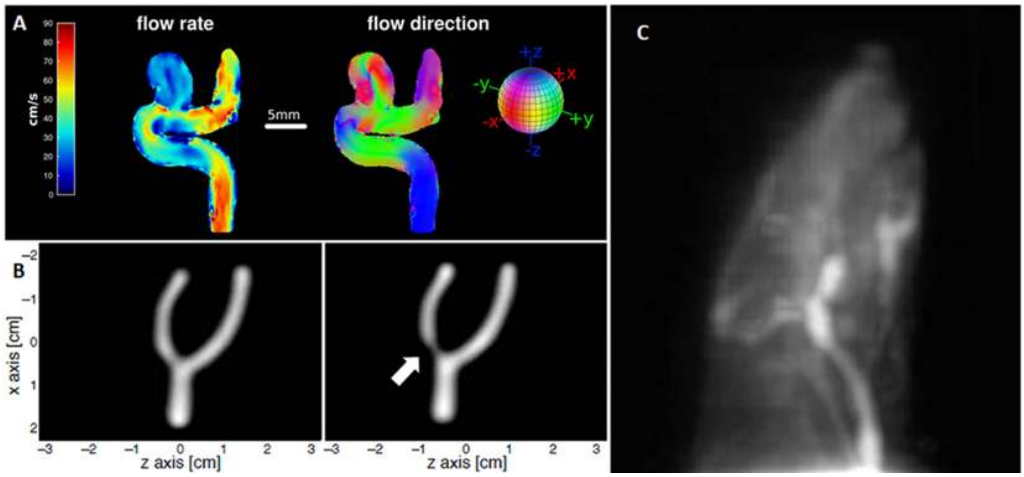

diagnosis. Tc99m or In111 radioisotopes-labeled innate white blood cells (WBCs) have been used for clinical diagnosis of inflammation, infection and fever of unknown origin.[57,58] RBC labeled with radioisotopes have been used as a blood pool agent for the diagnosis of vascular defects.[59] Chromosomal aberration resulting from labeling cells with radioisotopes is a big concern.[60] While cell tracking with MRI is useful, the negative contrast T_2* imaging could be a confound in tissues such as lung, bone and tendon and thus limits the inherent sensitivity of the technique to approximately ~10,000 labeled cells.[61] Table 2 compares the advantages and disadvantages of various preclinical modalities used for cell tracking. In contrast to existing modalities, MPI offers high sensitivity radiation-free labeling, with no (radioactive) decay of signal over time that is very helpful for longitudinal studies.

The MR-cell tracking literature has already shown a good safety profile for labeling immune cells[63,64] or stem cells[65–67] with SPIOs.[68] In a recent MPI study by Zheng B et al (Figure 6), 200 cell detection sensitivity was reported using a 2.35 T m^{-1} field-free line projection MPI scanner, the highest sensitivity achieved among all imaging modalities based on a review reported by Nguyen PK et al.[61] MPI's superior sensitivity, the absence of background signal, the safety profile of the tracer and ability to image at depth, makes the technique extremely valuable for cell tracking applications. Currently, various cell-based therapeutics are being investigated, including stem cells, chimeric antigen receptor T-cells , and dendritic cell vaccines. Cell tracking is essential especially for monitoring the fate of cell-based therapeutics, their biodistribution and clearance, and in identifying patients as responders or non-responders.[70] Another key interest is to find out whether the administered cells proliferate and are alive or dead.[71] Intracellular viscosity measurement of SPIO-labeled cells using MPI, *e.g.* can enable to distinguish live *vs* dead cells in the graft.[72,73] Fidler F et al linked the changes in magnetic particle harmonic-spectrum over time to the viability of the stem cell, comparing live cells with internalized SPIOs to dying cells in the process of lysis where SPIOs are released.[74] Fidler attributed the spectral changes because of change in Brownian relaxation behavior of the SPIO during the lysis process.

Table 2. Comparison of pre-clinical cell tracking methods, data adapted and modified from,[5,61,62] we noted that Ultrasound and CT are not well characterized for tracking cells

Modality	Resolution	Acquisition speed	Sensitivity/cells detected	Cell labeling agents
Optical	20 μm/poor at depth	<Seconds	μM/1000	Reporter gene/dyes (IcG, Cy, Luciferase)
Nuclear medicine	1000–2000 μm	Minutes	pM/10,000–100,000	Radionuclide (In111, Tc99m, 18F, 68Ga)
MRI	25–500 μm	Minutes	mM/10,000	Contrast agent (Gd, Mn, SPIO, 19F)
MPI	*250–1400 μm*	*Minutes*	*0.1 μM/10–200*	*SPIO*

MPI, magnetic particle imaging; SPIO, superparamagnetic iron oxide nanoparticle.

Figure 6. Tracking of SPIO-labeled cells provide vital information in regenerative medicine. (A) 87 days of tracking SPIO-tagged NPCs in the forebrain of a rodent. The labeled cells migrated into the ventricle of the brain (B) as shown by Prussian blue staining of SPIO-labeled cells (Figure adopted with permission from Zheng B et al[5] Springer Nature). (C) MPI image of SPIO-labeled pancreatic islet cells transplanted under the kidney capsule; the transplanted labeled cells were functional as indicated by (D) immunofluorescence staining (red, insulin; green, dextran, blue, cell nucleus) (Reproduced with permission from[69]). MPI, magnetic particle imaging; NPC, neuronal progenitor cell; SPIO, super paramagnetic iron oxide nanoparticle.

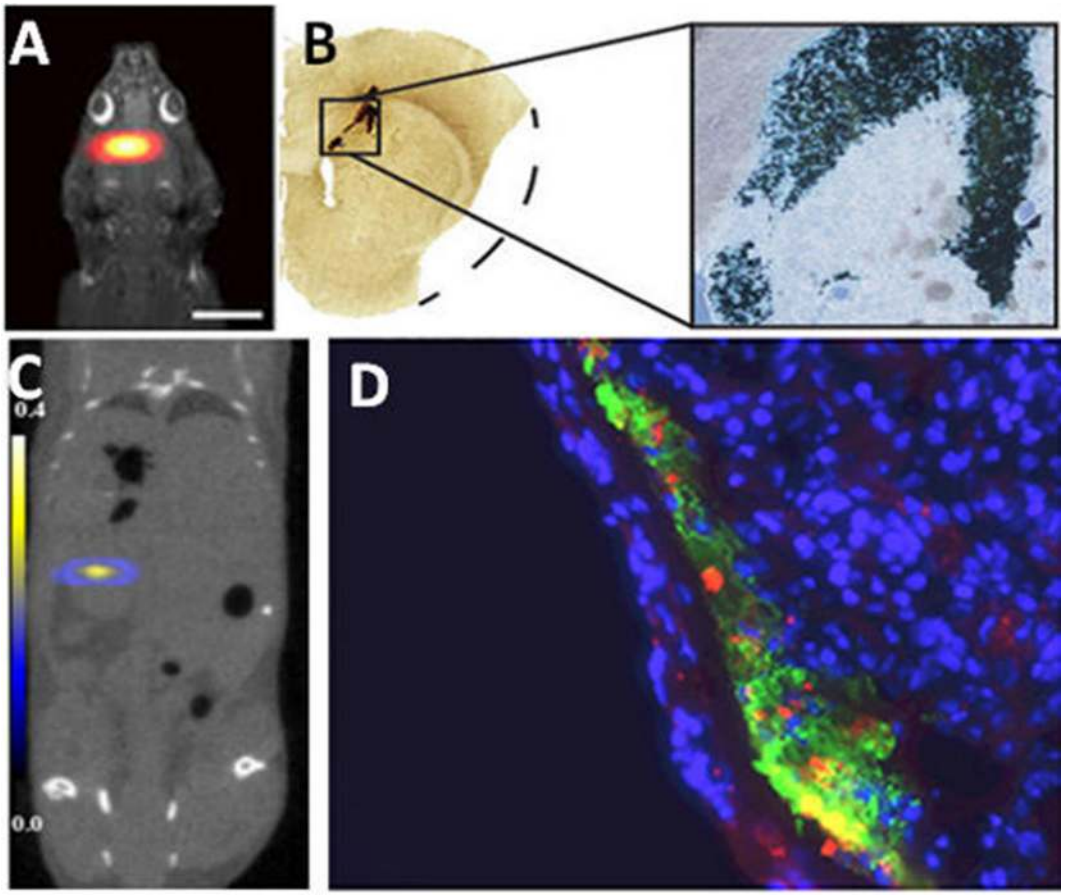

Figure 7. MPI can be used as a theranostic platform, for diagnosis and treatment of cancer using hyperthermia.[79–81] MPI enables image-guided therapy where a new approach of using the MPI gradient field to localize thermal dose deposition at-depth with margins of 7 mm using a 2.35 T m^{-1} gradient and 2 mm using a 7 T m^{-1} gradient. Using MPI images, Tay et al[79] (A) predicted the heat deposition to tumor, and by using gradients and high excitation frequency (B) was able to spatially-selectively deposit thermal dose in a phantom and in a dual tumor xenograft model, (C) where the bottom tumor was selectively treated but not the tumor in the top (Reproduced with permission from,[79] 2018 Copyright, American Chemical Society). MPI, magnetic particle imaging.

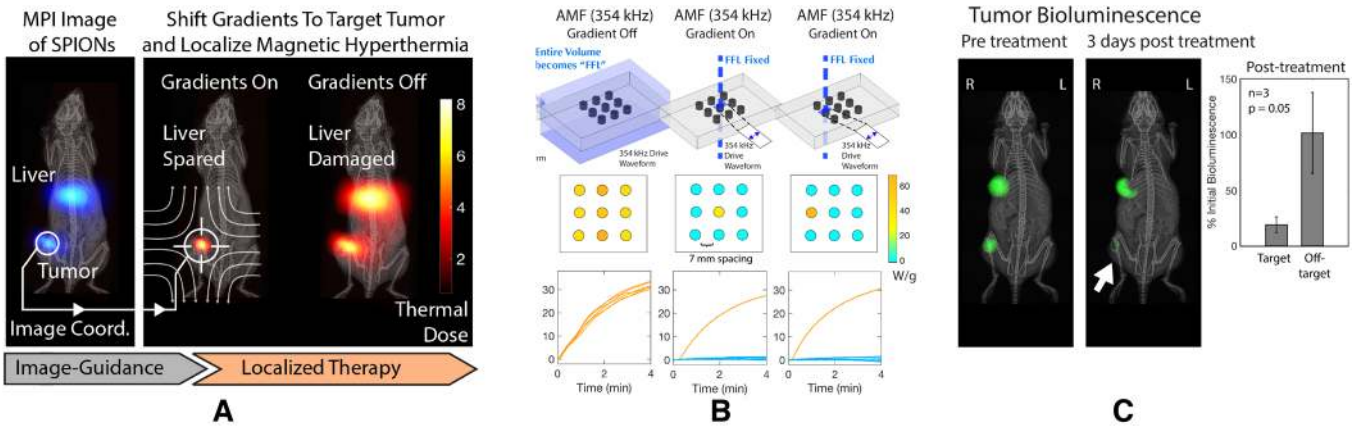

Figure 8. MPI sensitivity dependence on various parameters. Equation assumes limit of detection at SNR = 1 for a 1 s scan, and sensor coil noise dominance (body noise negligible and ideal noise matching to pre-amplifiers). Parameters: ρ = density of SPIO, k_B = Boltzmann constant, T = temperature of sensor coil, NF = noise figure of the preamplifier, R_{coil} = resistance of coil, B_{coil} = sensitivity of coil, H_{sat} = applied field H needed to achieve M_{sat}, M_{sat} = magnetization value at saturation, BW = final receive bandwidth used (after windowing), ω = 2π* excitation frequency, H_{ampl} = excitation amplitude. The derivation estimates peak dM/dt can be approximated by m_{sat}/(Δt necessary to go from H = 0 to H = H_{sat}), where m_{sat} = M_{sat}*$V_{nanoparticle}$, m represents magnetic moment. MPI, magnetic particle imaging; SNR, signal-to-noise ratio.

$$Limit\ of\ Detection \approx 2\rho\sqrt{k_B} \cdot \frac{NF\sqrt{T_{coil}R_{coil}}}{B_{coil}} \cdot \frac{H_{sat}}{M_{sat}} \cdot \frac{\sqrt{BW}}{\omega H_{ampl}}$$

Hardware Parameters | Nanoparticle Parameters | Scanning Parameters

In another recent study by Wang P et al, pancreatic islet cells were labeled with SPIOs and safely transplanted in a murine model (Figure 6), resulting in grafting and insulin secretion in these cells.[75] The authors believe, such an approach will enable clinicians to track the progress of transplanted organ or tissue and verify suitable visceral sites for islet survival.

MPI in theranostics and other applications

Magnetic hyperthermia for treating cancer has garnered interest worldwide due to its potential to deposit heat at any depth. With conventional hyperthermia systems, it is difficult to focus the thermal dose to a specific tissue and avoid non-specific damage (λ/2 ~ 50 m).[76]

The same principle of MPI can be modified to spatially select and deposit thermal dose in biological tissue. Tissue death can be brought about by heating the biological sample to 43°C, a process known as induced hyperthermia. MPI uses a low sinusoidal excitation frequency in the order of 20 kHz, but by exciting SPIO particles at a higher frequency of 300 kHz, heat can be generated.[77] Hensley et al demonstrated a method of spatially localizing thermal heat deposition using magnetic gradients, similar to the physics behind acquiring MPI images.[78] The field-free region (FFR) generated by the gradient magnet as described in the "Introduction" can control the excitation of iron oxide nanoparticle in space; the particles under the influence of the gradient magnet are locked, and the particles at the FFR are free to rotate, thereby, restricting the thermal dose deposition at the FFR alone. This principle was adopted by Tay et al *in vivo*.[79] Tay and team used the MPI image to quantify the concentration of iron and employed a forward model to predict the thermal dose (Figure 7), followed by selectively treating one tumor in a dual tumor murine model using induced hyperthermia. Using this approach, Tay and team could localize thermal dose deposition with a spatial resolution of 7 mm, and with no toxic effect to visceral organs such as the liver. More precise localization to <2.3 mm can be achieved by improving gradient from 2.35 to 7 T m^{-1}.

Figure 9. Future of MPI scanner. (A) An integrated MPI-MRI system designed by Bruker BioSpin GmbH and University of RWTH, Achen. Image shows a cavity phantom with MRI image in greyscale and MPI image rendered in red scale. (Adapted with permission from[105]) (B) A human scale head MPI scanner design demonstrating the FFL region using a *x-z* gradient of 1 T m^{-1} (Reproduced under the creative common license from[106]). (C) Magnetostimulation limit and SAR estimate in human torso (graph reproduced with permission from[107]), PNS is the dominant safety concern for MPI at drive field frequency <42 kHz. FFL, field-free line; MPI, magnetic particle imaging; PNS, peripheral nerve stimulation.

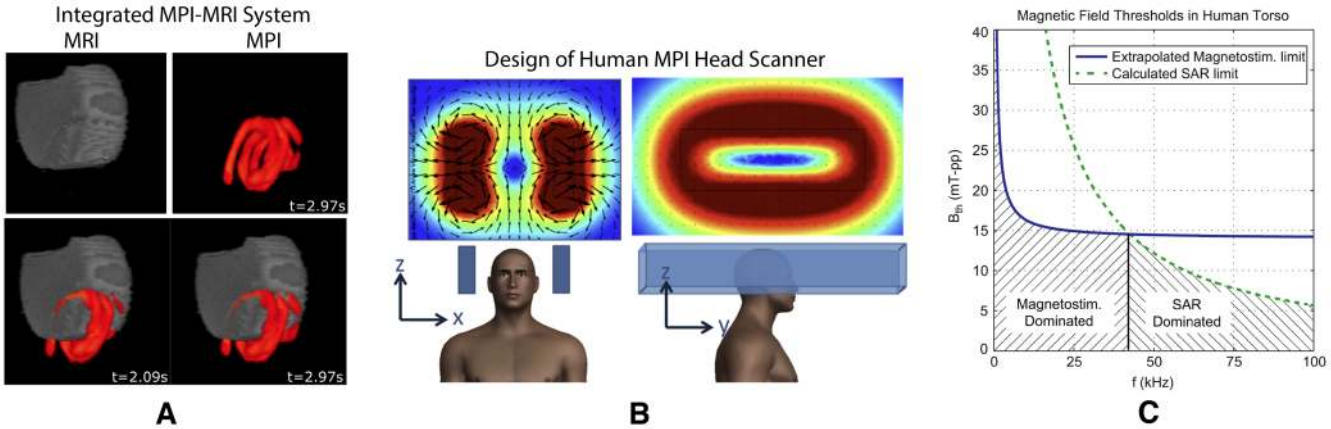

The treatment approach described above can also be extended for combinatorial therapy, in which a triggered release of an encapsulated drug can be achieved in combination with hyperthermia,[82] providing greater precision of treatment and reducing toxic effects. Further, MPI thermometry approaches can be explored to monitor the temperature rise during hyperthermia.[23,24]

MPI is also an invaluable tool for studying neuronal responses in brain to external stimuli. Neuronal response is associated with increased metabolism of the neuron followed by an intrinsic signal relay between the vasculature and neuronal activity. Changes associated with cerebral blood volume (CBV) and cerebral blood perfusion have been the basis of functional brain imaging. CBV changes resulting from neurovascular coupling can be directly measured as a change in the tracer signal from the blood vessel. In the pioneering work, Orendorff R et al performed the first CBV measurement in rodent brain using MPI by bolus tracking of SPIO particles administered intravenously.[83] CBV measurement using MPI can be a sensitive tool for studying brain function.[84,85]

TRANSLATION OF MPI TO HUMAN SCALE

MPI has grown rapidly in recent years, and clinical translation on the horizon. Recent developments in the field are anticipated to ease this translation significantly.

Specific absorption rate (SAR) limits

Like MRI, MPI must address safety issues such as magnetostimulation and tissue heating as measured by SAR since it also exposes the human body to time-varying magnetic fields (excitation field). Saritas et al[86] has performed an in-depth analysis on this subject with human data and shown that it is possible to maintain safety when scaling up to human size if certain MPI excitation limits are observed. These limits negligibly affect MPI sensitivity when scaling-up, since the required reduction in excitation amplitude is compensated by a possible increase in excitation frequency,[87] since current preclinical MPI uses very low frequencies (~20 kHz). Interestingly, recent work has shown that low excitation (drive) amplitude actually improves MPI spatial resolution,[88] and thus, a human-compatible MPI excitation sequence should perform at least equally well as current preclinical MPI excitation sequences.

Hardware scale up

In addition, it is critical to discuss challenges facing MPI hardware in scaling-up from pre-clinical to human size. Scaling will involve increased power requirement and cost. Current MPI pre-clinical scanners are able to produce a high gradient field of 6.3 T m^{-1}.[6] Of course, MPI resolution scales directly with gradient strength.[14] But no MPI scanner today uses superconducting gradients, but as with MRI scanners, a superconducting gradient may be cost-effective for human MPI. Pre-clinical MPI imaging scanners have used NdFeB permanent magnets[89] or laminated iron return electromagnets for more modern field-free line scanners.[90] Cryogen-free magnets using compact cryocoolers and high temperature superconductors (HTS) with active shielding and parts per million (ppm) field homogeneities have been developed for head MRI,[91,92] to reduce operational costs. MRI scanners require stringent, 1 ppm field uniformity. Fortunately, MPI scanners can tolerate more than 1–5% field inhomogeneity while producing artifact-free images.[89] This basic physics attribute of MPI explains why scans are perfectly robust in the lungs where air in the alveolar sacs produces 9 ppm field variations in the tissue. These intense field gradients cause short T_2^*, making lung MRI very challenging. By contrast, MPI of the lung is completely robust, as shown in various studies.[5,45,62,93] It is worth noting that the 7 T m^{-1} gradients employed in pre-clinical MPI are already an everyday experience for patients, as clinical 3 T MRI scanners have a 7.2 T m^{-1} maximum spatial gradient just outside the bore.[4,94]

SPIO optimization

A very promising approach to human MPI is to develop better MPI-tailored SPIOs with sharper magnetization curves. For instance, improving the phase purity of the SPIO tracer as shown by University of Washington/Lodespin Labs resulted in better MPI spatial resolution. These SPIOs have been shown to have almost two-fold better spatial resolution than Resovist™ in reconstructed MPI images.[95,96] We anticipate that further optimization of the SPIO for MPI imaging can achieve further gains in spatial resolution that can be traded-off for lower MPI gradients to ease hardware scaling-up to human size. For example, a 10-fold improvement in resolution due to a sharper Langevin saturation curve could reduce the gradient cost by up to 100-fold, which could be enabling. Regulatory approval of new MPI tracers should be similar to the established approvals of MRI SPIO tracers, like Feraheme® or Resovist® or other iron oxide-based T_1 or T_2^* tracers. Future MPI tracers could be approved through three pathways: (a) as tracer for tracking cell therapy (b) new diagnostic applications, and (c) theranostic applications. Each pathway requires a different Food and Drug Administration (FDA) approval, and may require a designation as an investigational new drug (IND). Specifically, MPI tracers for vascular imaging or lymph node imaging will require FDA approval as a new tracer agent consideration for imaging indication. In comparison, MPI tracers for cell tracking will require an IND as a cell therapy product. Finally, tracers for theranostics will require specialized consideration depending on the overall survival benefit of treatment. The FDA has non-binding guidelines of preclinical studies and safety assessment set forth before an IND can enter clinical trials.[97]

Theoretical sensitivity limits of MPI

Finally, MPI is still a new field, and current scanner performance limits do not represent the physical performance limits of MPI. For example, MRI hardware has reached body noise dominance, but due to the very low frequencies used in MPI, so radiofrequency coil sensor improvements are challenging. However, because today's MPI receiver coils operate a low frequency (<5 MHz) and are small diameter (preclinical), the coil noise dominates the body noise.[7,98] This means there is substantial room for technical advances in MPI sensitivity.

From prior work,[7,99] MPI's limit of detection can be approximated as shown in Figure 8.

Prior theoretical work on human MPI[99] predicted MPI sensitivity as 5 pg in a 1 s scan (65 nM in a 1 mm^3 voxel). However, optimization of receive hardware (such as 77K cryogenic litz/high temperature superconductors receive coils,[100–102] MPI-tailored SPIOs with very small H_{sat} and optimized scanning sequences/digital bandwidth windowing could potentially improve each parameter-group in the Figure 8 equation, and in combination potentially improve SNR by orders of magnitude.

CONCLUSION

MPI has grown out of its infancy, and tremendous progress is being made in the pre-clinical space using this safe and sensitive imaging modality.[8,103] A clinical MPI scanner is not far from reality. Progress has been made on multimodal imaging with MPI such as X-ray, CT and MRI.[104] Recently, a preclinical highly integrated hybrid MPI-MRI system was developed[105] (Figure 9). Another exciting area of research is MPI-tailored SPIOs which have already shown improved MPI resolution and sensitivity and could be further improved. With several promising translatable approaches and superior safety profile of MPI tracers, we are hopeful that MPI will play a crucial role as a clinical diagnostic and nanotheranostic tool in the near future.

ACKNOWLEDGMENT

We acknowledge support from NIH Grants R01 EB019458 and EB024578, UC TRDRP Grant 26IP-0049, M. Cook Chair and the UC Discovery Award. We also acknowledge the fellowship support from the Siebel Scholars Foundation and the Agency of Science Technology and Research, Singapore (ZWT).

COMPETING INTERESTS

The authors declare the following competing financial interest(s): Dr P. Goodwill and Prof S. Conolly hold equity interest in Magnetic Insight, Inc. In addition, Dr P. Goodwill, Dr E. Yu, Dr R. Orendorff and Dr D. Hensley receive income from Magnetic Insight, Inc.

REFERENCES

1. Gleich B, Weizenecker J. Tomographic imaging using the nonlinear response of magnetic particles. *Nature* 2005; **435**: 1214–7. doi: https://doi.org/10.1038/nature03808
2. Knopp T, Gdaniec N, Möddel M. Magnetic particle imaging: from proof of principle to preclinical applications. *Physics in Medicine & Biology* 2017; **62**: R124–R178. doi: https://doi.org/10.1088/1361-6560/aa6c99
3. Konkle JJ, Goodwill PW, Carrasco-Zevallos OM, Conolly SM. Projection reconstruction magnetic particle imaging. *IEEE Trans Med Imaging* 2013; **32**: 338–47. doi: https://doi.org/10.1109/TMI.2012.2227121
4. Saritas EU, Goodwill PW, Croft LR, Konkle JJ, Lu K, Zheng B, et al. Magnetic Particle Imaging (MPI) for NMR and MRI researchers. *J Magn Reson* 2013; **229**: 116–26. doi: https://doi.org/10.1016/j.jmr.2012.11.029
5. Zheng B, Vazin T, Goodwill PW, Conway A, Verma A, Saritas EU, et al. Magnetic Particle Imaging tracks the long-term fate of in vivo neural cell implants with high image contrast. *Sci Rep* 2015; **5**: 14055. doi: https://doi.org/10.1038/srep14055
6. Yu EY, Chandrasekharan P, Berzon R, Tay ZW, Zhou XY, Khandhar AP, et al. Magnetic particle imaging for highly sensitive, quantitative, and safe in vivo gut bleed detection in a murine model. *ACS Nano* 2017; **11**: 12067–76. doi: https://doi.org/10.1021/acsnano.7b04844
7. Goodwill PW, Conolly SM. The X-space formulation of the magnetic particle imaging process: 1-D signal, resolution, bandwidth, SNR, SAR, and magnetostimulation. *IEEE Trans Med Imaging* 2010; **29**: 1851–9. doi: https://doi.org/10.1109/TMI.2010.2052284
8. Zheng B, Yu E, Orendorff R, Lu K, Konkle JJ, Tay ZW, et al. Seeing SPIOs directly in vivo with magnetic particle imaging. *Mol Imaging Biol* 2017; **19**: 385–90. doi: https://doi.org/10.1007/s11307-017-1081-y
9. Goodwill PW, Saritas EU, Croft LR, Kim TN, Krishnan KM, Schaffer DV, et al. X-space MPI: magnetic nanoparticles for safe medical imaging. *Adv Mater* 2012; **24**: 3870–7. doi: https://doi.org/10.1002/adma.201200221
10. Goodwill PW, Conolly SM. The X-space formulation of the magnetic particle imaging process: 1-D signal, resolution, bandwidth, SNR, SAR, and magnetostimulation. *IEEE Trans Med Imaging* 2010; **29**: 1851–9. doi: https://doi.org/10.1109/TMI.2010.2052284
11. Goodwill PW, Konkle JJ, Zheng B, Conolly SM, Conolly SM. Projection x-space magnetic particle imaging. *IEEE Trans Med Imaging* 2012; **31**: 1076–85. doi: https://doi.org/10.1109/TMI.2012.2185247
12. Rahmer J, Weizenecker J, Gleich B, Borgert J. Signal encoding in magnetic particle imaging: properties of the system function. *BMC Med Imaging* 2009; **9**: 4. doi: https://doi.org/10.1186/1471-2342-9-4
13. Gilchrist RK, Medal R, Shorey WD, Hanselman RC, Parrott JC, Taylor CB. Selective inductive heating of lymph nodes. *Ann Surg* 1957; **146**: 596–606. doi: https://doi.org/10.1097/00000658-195710000-00007
14. Zhi Wei T, Daniel WH, Erika CV, Bo Z, Steven MC. The relaxation wall: experimental limits to improving MPI spatial resolution by increasing nanoparticle core size. *Biomedical Physics & Engineering Express* 2017; **3**: 035003.
15. Lawaczeck R, Bauer H, Frenzel T, Hasegawa M, Ito Y, Kito K, et al. Magnetic iron oxide particles coated with carboxydextran for parenteral administration and liver contrasting. Pre-clinical profile of SH U555A. *Acta Radiol* 1997; **38**(4 Pt 1): 584–97.
16. Daldrup-Link HE, Golovko D, Ruffell B, Denardo DG, Castaneda R, Ansari C, et al. MRI of tumor-associated macrophages with clinically applicable iron oxide nanoparticles. *Clin Cancer Res* 2011; **17**: 5695–704. doi: https://doi.org/10.1158/1078-0432.CCR-10-3420
17. Balakrishnan VS, Rao M, Kausz AT, Brenner L, Pereira BJG, Frigo TB, et al. Physicochemical properties of ferumoxytol, a new intravenous iron preparation. *Eur J Clin Invest* 2009; **39**: 489–96. doi: https://doi.org/10.1111/j.1365-2362.2009.02130.x
18. Saeed M, Wendland MF, Engelbrecht M, Sakuma H, Higgins CB. Value of blood pool contrast agents in magnetic resonance angiography of the pelvis and lower extremities. *Eur Radiol* 1998; **8**: 1047–53. doi: https://doi.org/10.1007/s003300050512
19. Keselman P, Yu EY, Zhou XY, Goodwill PW, Chandrasekharan P, Ferguson RM, et al. Tracking short-term biodistribution and long-term clearance of SPIO tracers in magnetic particle imaging. *Phys Med Biol*

2017; **62**: 3440–53. doi: https://doi.org/10.1088/1361-6560/aa5f48
20. Tay ZW, Goodwill PW, Hensley DW, Taylor LA, Zheng B, Conolly SM. A high-throughput, arbitrary-waveform, MPI spectrometer and relaxometer for comprehensive magnetic particle optimization and characterization. *Sci Rep* 2016; **6**: 34180. doi: https://doi.org/10.1038/srep34180
21. Murase K, Song R, Hiratsuka S. Magnetic particle imaging of blood coagulation. *Appl Phys Lett* 2014; **104**: 252409. doi: https://doi.org/10.1063/1.4885146
22. Utkur M, Muslu Y, Saritas EU. Relaxation-based viscosity mapping for magnetic particle imaging. *Phys Med Biol* 2017; **62**: 3422–39. doi: https://doi.org/10.1088/1361-6560/62/9/3422
23. Weaver JB, Rauwerdink AM, Hansen EW. Magnetic nanoparticle temperature estimation. *Med Phys* 2009; **36**: 1822–9. doi: https://doi.org/10.1118/1.3106342
24. Stehning C, Gleich B, Rahmer J. Simultaneous magnetic particle imaging (MPI) and temperature mapping using multi-color MPI. *IJMPI* 2016. 2016; **2**.
25. Hensley D, Goodwill P, Croft L, Conolly S. Preliminary experimental X-space color MPI. 2015 5th International Workshop on Magnetic Particle Imaging (IWMPI); 2015.
26. Rahmer J, Halkola A, Gleich B, Schmale I, Borgert J. First experimental evidence of the feasibility of multi-color magnetic particle imaging. *Phys Med Biol* 2015; **60**: 1775–91. doi: https://doi.org/10.1088/0031-9155/60/5/1775
27. Rahmer J, Wirtz D, Bontus C, Borgert J, Gleich B. Interactive magnetic catheter steering with 3-D real-time feedback using multi-color magnetic particle imaging. *IEEE Trans Med Imaging* 2017; **36**: 1449–56. doi: https://doi.org/10.1109/TMI.2017.2679099
28. Weissleder R, Stark DD, Engelstad BL, Bacon BR, Compton CC, White DL, et al. Superparamagnetic iron oxide: pharmacokinetics and toxicity. *AJR* 1989; **152**: 167–73. doi: https://doi.org/10.2214/ajr.152.1.167
29. Hilty FM, Arnold M, Hilbe M, Teleki A, Knijnenburg JTN, Ehrensperger F, et al. Iron from nanocompounds containing iron and zinc is highly bioavailable in rats without tissue accumulation. *Nat Nanotechnol* 2010; **5**: 374–80. doi: https://doi.org/10.1038/nnano.2010.79
30. Reimer P, Balzer T. Ferucarbotran (Resovist): a new clinically approved RES-specific contrast agent for contrast-enhanced MRI of the liver: properties, clinical development, and applications. *Eur Radiol* 2003; **13**: 1266–76. doi: https://doi.org/10.1007/s00330-002-1721-7
31. Zinderman CE, Landow L, Wise RP. Anaphylactoid reactions to Dextran 40 and 70: Reports to the United States Food and Drug Administration, 1969 to 2004. *J Vasc Surg* 2006; **43**: 1004–9. doi: https://doi.org/10.1016/j.jvs.2006.01.006
32. Wang Y-XJ, Hussain SM, Krestin GP. Superparamagnetic iron oxide contrast agents: physicochemical characteristics and applications in MR imaging. *Eur Radiol* 2001; **11**: 2319–31. doi: https://doi.org/10.1007/s003300100908
33. Ferguson RM, Khandhar AP, Kemp SJ, Arami H, Saritas EU, Croft LR, et al. Magnetic particle imaging with tailored iron oxide nanoparticle tracers. *IEEE Trans Med Imaging* 2015; **34**: 1077–84. doi: https://doi.org/10.1109/TMI.2014.2375065
34. Chou C-T, Chen R-C, Chen W-T, Lii J-M. Percentage of signal intensity loss for characterisation of focal liver lesions in patients with chronic liver disease using ferucarbotran-enhanced MRI. *Br J Radiol* 2010; **83**: 1023–8. doi: https://doi.org/10.1259/bjr/21476692
35. Golovko DM, Henning T, Bauer JS, Settles M, Frenzel T, Mayerhofer A, et al. Accelerated stem cell labeling with ferucarbotran and protamine. *Eur Radiol* 2010; **20**: 640–8. doi: https://doi.org/10.1007/s00330-009-1585-1
36. Schwenk MH. Ferumoxytol: a new intravenous iron preparation for the treatment of iron deficiency anemia in patients with chronic kidney disease. *Pharmacotherapy* 2010; **30**: 70–9. doi: https://doi.org/10.1592/phco.30.1.70
37. Anselmo AC, Mitragotri S. Nanoparticles in the clinic. *Bioeng Transl Med* 2016; **1**: 10–29. doi: https://doi.org/10.1002/btm2.10003
38. Vasanawala SS, Nguyen K-L, Hope MD, Bridges MD, Hope TA, Reeder SB, et al. Safety and technique of ferumoxytol administration for MRI. *Magn Reson Med* 2016; **75**: 2107–11. doi: https://doi.org/10.1002/mrm.26151
39. Ruangwattanapaisarn N, Hsiao A, Vasanawala SS. Ferumoxytol as an off-label contrast agent in body 3T MR angiography: a pilot study in children. *Pediatr Radiol* 2015; **45**: 831–9. doi: https://doi.org/10.1007/s00247-014-3226-3
40. Namkung S, Zech CJ, Helmberger T, Reiser MF, Schoenberg SO. Superparamagnetic iron oxide (SPIO)-enhanced liver MRI with ferucarbotran: efficacy for characterization of focal liver lesions. *J Magn Reson Imaging* 2007; **25**: 755–65. doi: https://doi.org/10.1002/jmri.20873
41. Tokunaga S, Koda M, Matono T, Sugihara T, Nagahara T, Ueki M, et al. Assessment of ablative margin by MRI with ferucarbotran in radiofrequency ablation for liver cancer: comparison with enhanced CT. *Br J Radiol* 2012; **85**: 745–52. doi: https://doi.org/10.1259/bjr/64518148
42. Wu L, Cao Y, Liao C, Huang J, Gao F. Diagnostic performance of USPIO-enhanced MRI for lymph-node metastases in different body regions: A meta-analysis. *Eur J Radiol* 2011; **80**: 582–9. doi: https://doi.org/10.1016/j.ejrad.2009.11.027
43. Pouw JJ, Grootendorst MR, Bezooijen R, Klazen CAH, De Bruin WI, Klaase JM, et al. Pre-operative sentinel lymph node localization in breast cancer with superparamagnetic iron oxide MRI: the SentiMAG Multicentre Trial imaging subprotocol. *Br J Radiol* 2015; **88**: 20150634. doi: https://doi.org/10.1259/bjr.20150634
44. Fortuin AS, Brüggemann R, van der Linden J, Panfilov I, Israël B, Scheenen TWJ, et al. Ultra-small superparamagnetic iron oxides for metastatic lymph node detection: back on the block. *Wiley Interdiscip Rev Nanomed Nanobiotechnol* 2018; **10**: e1471. doi: https://doi.org/10.1002/wnan.1471
45. Xinyi YZ, Kenneth EJ, Elaine YY, Bo Z, Patrick WG, Payam N, et al. First in vivo magnetic particle imaging of lung perfusion in rats. *Physics in Medicine & Biology* 2017; **62**: 3510.
46. Ludewig P, Gdaniec N, Sedlacik J, Forkert ND, Szwargulski P, Graeser M, et al. Magnetic particle imaging for real-time perfusion imaging in acute stroke. *ACS Nano* 2017; **11**: 10480–8. doi: https://doi.org/10.1021/acsnano.7b05784
47. Maeda H. The enhanced permeability and retention (EPR) effect in tumor vasculature: the key role of tumor-selective macromolecular drug targeting. *Adv Enzyme Regul* 2001; **41**: 189–207. doi: https://doi.org/10.1016/S0065-2571(00)00013-3
48. Miller MA, Arlauckas S, Weissleder R. Prediction of anti-cancer nanotherapy efficacy by imaging. *Nanotheranostics* 2017; **1**: 296–312. doi: https://doi.org/10.7150/ntno.20564
49. Yu EY, Bishop M, Zheng B, Ferguson RM, Khandhar AP, Kemp SJ, et al. Magnetic particle imaging: a novel in vivo imaging platform for cancer detection. *Nano Lett* 2017; **17**: 1648–54. doi: https://doi.org/10.1021/acs.nanolett.6b04865
50. Deo A, Fogel M, Cowper SE. Nephrogenic systemic fibrosis: a population study examining the relationship of disease development to gadolinium exposure. *Clin J*

Am Soc Nephrol 2007; **2**: 264–7. doi: https://doi.org/10.2215/CJN.03921106
51. Cheong BY, Muthupillai R. Nephrogenic systemic fibrosis: a concise review for cardiologists. *Tex Heart Inst J* 2010; **37**: 508–15.
52. Sedlacik J, Frölich A, Spallek J, Forkert ND, Faizy TD, Werner F, et al. Magnetic particle imaging for high temporal resolution assessment of aneurysm hemodynamics. *PLoS One* 2016; **11**: e0160097. doi: https://doi.org/10.1371/journal.pone.0160097
53. Lu K, Goodwill PW, Saritas EU, Zheng B, Conolly SM. Linearity and shift invariance for quantitative magnetic particle imaging. *IEEE Trans Med Imaging* 2013; **32**: 1565–75. doi: https://doi.org/10.1109/TMI.2013.2257177
54. Zheng B, Lu K, Konkle JJ, Hensley DW, Keselman P, Orendorff RD. Magnetic Particle Imaging. In: Bulte JWM, Modo MMJ, eds. *Design and Applications of Nanoparticles in Biomedical Imaging*: Springer; 2017. pp. 69–93.
55. Markov DE, Boeve H, Gleich B, Borgert J, Antonelli A, Sfara C, et al. Human erythrocytes as nanoparticle carriers for magnetic particle imaging. *Phys Med Biol* 2010; **55**: 6461–73. doi: https://doi.org/10.1088/0031-9155/55/21/008
56. Rahmer J, Antonelli A, Sfara C, Tiemann B, Gleich B, Magnani M, et al. Nanoparticle encapsulation in red blood cells enables blood-pool magnetic particle imaging hours after injection. *Phys Med Biol* 2013; **58**: 3965–77. doi: https://doi.org/10.1088/0031-9155/58/12/3965
57. Lewis SS, Cox GM, Stout JE. Clinical Utility of Indium 111-Labeled White Blood Cell Scintigraphy for Evaluation of Suspected Infection. *Open Forum Infect Dis* 2014; **1**: ofu089: ofu089: . doi: https://doi.org/10.1093/ofid/ofu089
58. Becker W. The contribution of nuclear medicine to the patient with infection. *Eur J Nucl Med* 1995; **22**: 1195–211. doi: https://doi.org/10.1007/BF00800606
59. Srivastava SC, Rao Chervu L, Chervu LR. Radionuclide-labeled red blood cells: current status and future prospects. *Semin Nucl Med* 1984; **14**: 68–82. doi: https://doi.org/10.1016/S0001-2998(84)80022-7
60. ten Berge RJ, Natarajan AT, Hardeman MR, van Royen EA, Schellekens PT. Labeling with indium-111 has detrimental effects on human lymphocytes: concise communication. *J Nucl Med* 1983; **24**: 615–20.
61. Nguyen PK, Riegler J, Wu JC. Stem cell imaging: from bench to bedside. *Cell Stem Cell* 2014; **14**: 431–44. doi: https://doi.org/10.1016/j.stem.2014.03.009
62. Zheng B, von See MP, Yu E, Gunel B, Lu K, Vazin T, et al. Quantitative magnetic particle imaging monitors the transplantation, biodistribution, and clearance of stem cells *In Vivo*. *Theranostics* 2016; **6**: 291–301. doi: https://doi.org/10.7150/thno.13728
63. Richards JM, Shaw CA, Lang NN, Williams MC, Semple SI, MacGillivray TJ, et al. In vivo mononuclear cell tracking using superparamagnetic particles of iron oxide: feasibility and safety in humans. *Circ Cardiovasc Imaging* 2012; **5**: 509–17. doi: https://doi.org/10.1161/CIRCIMAGING.112.972596
64. de Vries IJ, Lesterhuis WJ, Barentsz JO, Verdijk P, van Krieken JH, Boerman OC, et al. Magnetic resonance tracking of dendritic cells in melanoma patients for monitoring of cellular therapy. *Nat Biotechnol* 2005; **23**: 1407–13. doi: https://doi.org/10.1038/nbt1154
65. Mahmoudi M, Hosseinkhani H, Hosseinkhani M, Boutry S, Simchi A, Journeay WS, et al. Magnetic resonance imaging tracking of stem cells in vivo using iron oxide nanoparticles as a tool for the advancement of clinical regenerative medicine. *Chem Rev* 2011; **111**: 253–80. doi: https://doi.org/10.1021/cr1001832
66. Zhu J, Zhou L, XingWu F. Tracking neural stem cells in patients with brain trauma. *N Engl J Med* 2006; **355**: 2376–8. doi: https://doi.org/10.1056/NEJMc055304
67. Bulte JW, Walczak P, Janowski M, Krishnan KM, Arami H, Halkola A, et al. Quantitative "Hot Spot" imaging of transplanted stem cells using superparamagnetic tracers and magnetic particle imaging (MPI). *Tomography* 2015; **1**: 91–7. doi: https://doi.org/10.18383/j.tom.2015.00172
68. Bulte JW. In vivo MRI cell tracking: clinical studies. *AJR Am J Roentgenol* 2009; **193**: 314–25. doi: https://doi.org/10.2214/AJR.09.3107
69. Wang P, Goodwill PW, Pandit P, Gaudet J, Ross A, Wang J, et al. Magnetic particle imaging of islet transplantation in the liver and under the kidney capsule in mouse models. *Quant Imaging Med Surg* 2018; **8**: 114–22. doi: https://doi.org/10.21037/qims.2018.02.06
70. Schroeder T. Imaging stem-cell-driven regeneration in mammals. *Nature* 2008; **453**: 345–51. doi: https://doi.org/10.1038/nature07043
71. Ahrens ET, Bulte JW. Tracking immune cells in vivo using magnetic resonance imaging. *Nat Rev Immunol* 2013; **13**: 755–63. doi: https://doi.org/10.1038/nri3531
72. Luby-Phelps K. Cytoarchitecture and Physical Properties of Cytoplasm: Volume, Viscosity, Diffusion, Intracellular Surface Area. In: Walter H, Brooks DE, Srere PA, eds. *International Review of Cytology*: Academic Press; 1999. pp. 189–221.
73. Utkur M, Muslu Y, Saritas EU. Relaxation-based viscosity mapping for magnetic particle imaging. *Phys Med Biol* 2017; **62**: 3422–39. doi: https://doi.org/10.1088/1361-6560/62/9/3422
74. Fidler F, Steinke M, Kraupner A, Grüttner C, Hiller K-H, Briel A, et al. Stem cell vitality assessment using magnetic particle spectroscopy. *IEEE Trans Magn* 2015; **51**: 1–4. doi: https://doi.org/10.1109/TMAG.2014.2337052
75. Wang P, Goodwill PW, Pandit P, Gaudet J, Ross A, Wang J, et al. Magnetic particle imaging of islet transplantation in the liver and under the kidney capsule in mouse models. *Quant Imaging Med Surg* 2018; **8**: 114–22. doi: https://doi.org/10.21037/qims.2018.02.06
76. Jha S, Sharma PK, Malviya R. Hyperthermia: role and risk factor for cancer treatment. *Achievements in the Life Sciences* 2016; **10**: 161–7. doi: https://doi.org/10.1016/j.als.2016.11.004
77. Dhavalikar R, Rinaldi C. Theoretical predictions for spatially-focused heating of magnetic nanoparticles guided by magnetic particle imaging field gradients. *J Magn Magn Mater* 2016; **419**: 267–73. doi: https://doi.org/10.1016/j.jmmm.2016.06.038
78. Daniel H, Zhi Wei T, Rohan D, Bo Z, Patrick G, Carlos R, et al. Combining magnetic particle imaging and magnetic fluid hyperthermia in a theranostic platform. *Physics in Medicine & Biology* 2017; **62**: 3483.
79. Tay ZW, Chandrasekharan P, Chiu-Lam A, Hensley DW, Dhavalikar R, Zhou XY, et al. Magnetic particle imaging-guided heating *in Vivo* using gradient fields for arbitrary localization of magnetic hyperthermia therapy. *ACS Nano* 2018; **12**: 3699–713. doi: https://doi.org/10.1021/acsnano.8b00893
80. Murase K, Aoki M, Banura N, Nishimoto K, Mimura A, Kuboyabu T, et al. Usefulness of magnetic particle imaging for predicting the therapeutic effect of magnetic hyperthermia. *OJMI* 2015; **5**: 15: 85: 99. doi: https://doi.org/10.4236/ojmi.2015.52013
81. Bauer LM, Situ SF, Griswold MA, Samia ACS. High-performance iron oxide nanoparticles for magnetic particle imaging – guided hyperthermia (hMPI). *Nanoscale* 2016; **8**: 12162–9. doi: https://doi.org/10.1039/C6NR01877G

82. Carregal-Romero S, Guardia P, Yu X, Hartmann R, Pellegrino T, Parak WJ. Magnetically triggered release of molecular cargo from iron oxide nanoparticle loaded microcapsules. *Nanoscale* 2015; **7**: 570–6. doi: https://doi.org/10.1039/C4NR04055D
83. Orendorff R, Wendland M, Yu E, Zheng B, Goodwill P, Conolly S.editors. First in vivo brain perfusion imaging using magnetic particle imaging. 2016; 2016 World Molecular Imaging Congress (WMIC 2016): Imaging Biology Improving Therapy], World Molecular Imaging Society (WMIS).
84. Ryan O, Austin JP, Bo Z, Shawn NS, Ferguson RM, Amit PK, et al. First in vivo traumatic brain injury imaging via magnetic particle imaging. *Physics in Medicine & Biology* 2017; **62**: 3501.
85. Cooley CZ, Mandeville JB, Mason EE, Mandeville ET, Wald LL. Rodent Cerebral Blood Volume (CBV) changes during hypercapnia observed using Magnetic Particle Imaging (MPI) detection. *Neuroimage* 2018;. doi: https://doi.org/10.1016/j.neuroimage.2018.05.004
86. Saritas E. U, Goodwill P. W, Zhang G. Z, Yu W, Conolly S. M et al. eds. *Magnetic Particle Imaging*. Berlin, Heidelberg: Springer Berlin Heidelberg; 2012 .
87. Gleich B. The Focus Field. In: Gleich B, ed. *Principles and Applications of Magnetic Particle Imaging*. Wiesbaden: Springer Fachmedien Wiesbaden; 2014. pp.. 45–7.
88. Croft LR, Goodwill PW, Konkle JJ, Arami H, Price DA, Li AX, , et al. Low drive field amplitude for improved image resolution in magnetic particle imaging. *Med Phys* 2016; **43**: 424–35. doi: https://doi.org/10.1118/1.4938097
89. Goodwill PW, Konkle JJ, Bo Zheng , Saritas EU, Conolly ST. Projection X-Space Magnetic Particle Imaging. *IEEE Trans Med Imaging* 2012; **31**: 1076–85. doi: https://doi.org/10.1109/TMI.2012.2185247
90. Goodwill P, Yu E, Conolly S, 2015. Design and construction of a second generation high-resolution MPI field free line scanner. 2015 5th International Workshop on Magnetic Particle Imaging (IWMPI).
91. Rybakov A, Bagdinov A, Demikhov E, Kostrov E, Lysenko V, Piskunov N, et al. 1.5 T cryogen free superconducting magnet for dedicated MRI. *IEEE Trans Appl Supercond* 2016; **26**: 1–3.
92. Razeti M, Angius S, Bertora L, Damiani D, Marabotto R, Modica M, et al. Construction and operation of cryogen Free MgB2 magnets for open MRI systems. *IEEE Trans Appl Supercond* 2008; **18**: 882–6. doi: https://doi.org/10.1109/TASC.2008.920661
93. Tay ZW, Chandrasekharan P, Zhou XY, EY Y, Zheng B, Conolly SM. In Vivo Tracking and Quantication of Inhaled Aerosol using Magnetic Particle Imaging towards Inhaled Therapeutic Monitoring. *Theranostics* 2018; **8**: 3676–87. doi: https://doi.org/10.7150/thno.26608
94. Shellock FG, Kanal E, Gilk TB. Regarding the value reported for the term "spatial gradient magnetic field" and how this information is applied to labeling of medical implants and devices. *AJR Am J Roentgenol* 2011; **196**: 142–5. doi: https://doi.org/10.2214/AJR.10.5004
95. Ferguson RM, Khandhar AP, Kemp SJ, Arami H, Saritas EU, Croft LR, et al. Magnetic particle imaging with tailored iron oxide nanoparticle tracers. *IEEE Trans Med Imaging* 2015; **34**: 1077–84. doi: https://doi.org/10.1109/TMI.2014.2375065
96. Hufschmid R, Arami H, Ferguson RM, Gonzales M, Teeman E, Brush LN, et al. Synthesis of phase-pure and monodisperse iron oxide nanoparticles by thermal decomposition. *Nanoscale* 2015; **7**: 11142–54. doi: https://doi.org/10.1039/C5NR01651G
97. Rieves D, Jacobs P. The use of published clinical study reports to support U.S. Food and Drug Administration approval of imaging agents. *J Nucl Med* 2016; **57**: 2022–6. doi: https://doi.org/10.2967/jnumed.116.178814
98. Macovski A. Noise in MRI. *Magn Reson Med* 1996; **36**: 494–7. doi: https://doi.org/10.1002/mrm.1910360327
99. Gleich B. Resolution, sensitivity and speed. In: Gleich B, ed. *Principles and Applications of Magnetic Particle Imaging*. Wiesbaden: Springer Fachmedien Wiesbaden; 2014. pp. 49–68.
100. Zheng B, Goodwill PW, Dixit N, Xiao D, Zhang W, Gunel B, et al. Optimal broadband noise matching to inductive sensors: application to magnetic particle imaging. *IEEE Trans Biomed Circuits Syst* 2017; **11**: 1041–52. doi: https://doi.org/10.1109/TBCAS.2017.2712566
101. QY M, Chan KC, Kacher DF, Gao E, Chow MS, Wong KK, et al. Superconducting RF coils for clinical MR imaging at low field. *Acad Radiol* 2003; **10**: 978–87.
102. Barral JK, Bangerter NK, Hu BS, Nishimura DG. In vivo high-resolution magnetic resonance skin imaging at 1.5 T and 3 T. *Magn Reson Med* 2010; **63**: 790–6. doi: https://doi.org/10.1002/mrm.22271
103. Zhou XY, Tay ZW, Chandrasekharan P, Yu EY, Hensley DW, Orendorff R, et al. Magnetic particle imaging for radiation-free, sensitive and high-contrast vascular imaging and cell tracking. *Curr Opin Chem Biol* 2018; **45**: 131–8. doi: https://doi.org/10.1016/j.cbpa.2018.04.014
104. Song G, Chen M, Zhang Y, Cui L, Qu H, Zheng X, et al. Janus Iron Oxides @ semiconducting polymer nanoparticle tracer for cell tracking by magnetic particle imaging. *Nano Lett* 2018; **18**: 182–9. doi: https://doi.org/10.1021/acs.nanolett.7b03829
105. Franke J, Heinen U, Lehr H, Weber A, Jaspard F, Ruhm W, et al. System characterization of a highly integrated preclinical hybrid MPI-MRI scanner. *IEEE Trans Med Imaging* 2016; **35**: 1993–2004. doi: https://doi.org/10.1109/TMI.2016.2542041
106. Mason EE, Cooley CZ, Cauley SF, Griswold MA, Conolly SM, Wald LL. Design analysis of an MPI human functional brain scanner. *Int J Magn Part Imaging* 2017; **3**. doi: https://doi.org/10.18416/ijmpi.2017.1703008
107. Saritas EU, Goodwill PW, Zhang GZ, Conolly SM. Magnetostimulation limits in magnetic particle imaging. *IEEE Trans Med Imaging* 2013; **32**: 1600–10. doi: https://doi.org/10.1109/TMI.2013.2260764